MJFAS
Malaysian Journal of Fundamental and Applied Sciences

Choirul *et al.* | Malaysian Journal of Fundamental and Applied Sciences, Vol. 20 (2024) 191-202

RESEARCH ARTICLE

Carbon-derived Black Soldier Fly (BSF) Larvae for Adsorption of Methylene Blue Dye: Characterization, Kinetic and Thermodynamic Studies

Muhamad Choirul[a], Mukhamad Nurhadi[a]*, Ratna Kusumawardani[a], Siti Anisa[a], Satifa Ananda Yulian[a], Siregar Aliya Rahma[a], Muhammad Akbar[a], Abdul Hamid Umar[b], Yubei Guo[c], Sin Yuan Lai[c,d]

[a]Department of Chemical Education, Universitas Mulawarman, Kampus Gunung Kelua, Samarinda, 75119, East Kalimantan, Indonesia; [b]Chemistry Department, Adamawa State University, Mubi PMB 25 Mubi, Adamawa State, Nigeria; [c]School of Energy and Chemical Engineering, Xiamen University Malaysia, Selangor Darul Ehsan 43900, Malaysia; [d]College of Chemistry and Chemical Engineering, Xiamen University, Xiamen 361005, China

Abstract The most effective substance for effectively adsorbing organic dyes is activated carbon (AC). We looked at the possibility of using Black Soldier Fly (BSF) larvae (Hermetia illucens Genome, MG) as a source for AC in this study. The two unique materials known as MG(300) and MG(500) were produced as a result of the larvae being heated for two hours at 300 and 500°C, respectively. These MG materials were further activated (MGO) using hydrogen peroxide (H_2O_2), and subsequently utilized for the adsorption of methylene blue (MB) dye. The objectives of this research include: (1) Investigation of the cabonization temperature and activation effects of the MG and MGO towards adsorption capacity; (2) Study of the physico-chemical properties of the adsorbents; (3) Exploration of the adsorptivity of MG and MGO in different parameters, including initial dye concentration, contact time, and temperature; (4) Examination of the kinetic and thermodynamic findings for the MG and MGO towards adsorption capacity. To analyze the obtained carbon, various analytical methods, including FTIR, WDXRF, SEM, and BET, were used. The equilibrium and kinetics of MB dye's adsorption behaviour on the AC were carefully investigated. It's interesting to note that within the first 10 minutes of contact time, all adsorbents demonstrated quick MB adsorption. The dye removal percentage (%) and adsorption capacities ($mg \cdot g^{-1}$) were measured at 65.7% and 6.33 $mg \cdot g^{-1}$ for MG(300), 76.5% and 11.07 $mg \cdot g^{-1}$ for MG(500), 91.1% and 16.41 $mg \cdot g^{-1}$ for MGO(300), and 96.1% and 17.13 $mg \cdot g^{-1}$ for MGO(500). Furthermore, the kinetics of dye adsorption using the pseudo-first-order (PFO) and pseudo-second-order (PSO) models were conducted, whereby PSO is the best fit with R^2 in the range of 0.949 to 0.999.

Keywords: Black soldier fly, adsorption, carbon, methylene blue, kinetics.

***For correspondence:**
mukh.nurhadi1969@gmail.com

Received: 17 Oct. 2023
Accepted: 1 Jan. 2024

Introduction

Insect species known as Black Soldier Fly (BSF) Larvae (Hermetia illucens) have the potential to replace soybean meal (SBM) in ruminant diets [1]. The most researched insect species is the black soldier fly (BSF), Hermetia illucens, whose larvae are raised on a massive scale all over the world. They are saprophytic insects that can consume animal manure and food scraps to make highly valuable animal protein meals. A huge biomass, diverse diet, high absorption and conversion rate, ease of care, and low cost of feeding were found due to their rapid reproduction [2-3]. The fly has the potential to be a novel and fruitful source of studied materials because it include a significant amount of chitin, a necessary component, of their exoskeleton, mouth parts and muscle attachment points [4]. Chitin, which is a viable material that can be transformed into carbon, has further revealed to have a high amount of carbon, 36.6 wt% [5]. Moreover, BSF larvae is a more sustainable alternative than sourcing the chitin vastly from waste of the fishing industry because it is not limited by the seasonal availability and high tolerance to a variety of pathogens[6]. The BSF larvae could valorise the animal

manure and food scraps to generate chitin as a carbon source, this demonstrating a further step in circular economy and environmental sustainability. The utilization of BSF larvae as a biosorbent for dye removal is enlightening.

Dye usage is common in the textile industry to give items colour. Nonetheless, these sectors face with a major difficulty with regard to wastewater treatment caused by dyes. This wastewater poses a major hazard to aquatic life, especially fish and other aquatic organisms, as it is loaded with a wide range of poisonous and organic chemicals [7]. Methylene blue (MB), a typical dye for dyeing cotton, wood, and silk, is frequently used as a model substance for the filtration of coloured and organic contaminants from aqueous solutions [8]. This dye has the potential to seriously irritate eyes and cause long-term injury to both people and animals. Ingestion of MB may result in a burning feeling and accompanying symptoms like nausea, vomiting, profuse sweating, and mental confusion. Whereas inhalation of MB may cause brief periods of rapid or laborious breathing [9]. Hence, treating effluents containing such dyes is paramount due to their adverse environmental implications.

Lately, there has been a lot of research being conducted on different methods for treating wastewater that contains dyes. These strategies include enhanced oxidation, photocatalytic degradation, flocculation [10], membrane filtration [11-12], and biodegradation [13], among other biological, chemical, and physical procedures. However, there are inherent disadvantages to these traditional treatments, including their high cost and complexity, which emphasize the need for simpler and more effective ways to treat wastewater containing dyes. Adsorption is the most advantageous of these techniques because of its many benefits, which include great efficacy, low cost, simplicity of use, and resistance to harmful compounds [14]. The most popular adsorbent for eliminating both organic and inorganic contaminants from water is activated carbon. BSF larvae with chitin abundance could serve as the source of activated carbon. Some researchers have employed enzymatic hydrolysis, acid hydrolysis, or acid and alkaline alcohol extraction to extract the chitin components [15]. Besides, another literature has adopted the modified exuviae of BSF larvae to adsorb bromophenol blue anionic dye [16].

To treat the dyes from the textile industry by using a circular economic and environmentally sustainable approach, this study explores the viability of using BSF larvae to produce AC as a promising material for MB dye adsorption. Furthermore, we assess its adsorption capacity and physico-chemical properties. It is worth noting that our work represents a novel contribution to this research field.

Materials and Methods

Carbonization Process

The larvae, referred to as MG, were sourced from the Animal Physiology Laboratory within the Faculty of Mathematics and Natural Sciences at the Universitas Mulawarman in East Kalimantan, Indonesia. These larvae were dehydrated by overnight exposure to 110 °C in an oven. The dehydrated larvae were carbonized in a furnace for two hours at two different temperatures, 300°C and 500°C, respectively, to produce carbon materials. The resulting carbon materials produced from the larvae at a specific temperature is denoted as MG(T). For instance, MG(500) represents the carbon material generated through the carbonization process carried out at 500°C for two hours.

Activation Process

Every 1 gram of MG was immersed in 10 mL of concentrated H_2O_2 (Merck). The mixture was stirred at room temperature for six hours and dried at 110 °C overnight. The MG that was activated is symbolized as MGO(T). For example, MGO(500) is AC that was immersed in concentrated H_2O_2 and prepared via the carbonization process at 500 °C for two hours.

Sample Characterization

Characterization of the sample employing various analytical techniques was conducted, including Wavelength Dispersive X-ray Fluorescence (WDXRF), Fourier Transform Infrared Spectroscopy (FTIR), Scanning Electron Microscopy (SEM), and Brunauer-Emmett-Teller (BET) adsorption-desorption.

To delve into the chemical composition of the crystal, we utilized a 1 kW Wavelength Dispersive X-ray Fluorescence (WDXRF) analyzer, specifically the PANalytical Minipal 4. The functional groups present in the samples were identified by subjecting them to analysis using an FTIR spectrometer, the Shimadzu IR-Prestige-21, with a spectral resolution of 2 cm^{-1}, scan duration of 10 seconds, at a

temperature of 20 °C, and a wavenumber range spanning from 400 to 4000 cm^{-1}.
For an in-depth exploration of the crystal's surface morphology, we employed the SEM (FEI Inspect S50) instrument, applying an accelerating voltage of 15 kV. Furthermore, nitrogen adsorption-desorption isotherms were acquired at a cryogenic temperature of -195.85°C and during an outgassing process at 300 °C. These measurements were conducted using the Quantachrome NovaWin instrument version 11.0.

Adsorption Test

The adsorption capabilities of our samples (ratio sample: dye = 0.0625 g: 25 mL) were evaluated using MB dye. Precisely, 0.0625 g of the adsorbent material were placed into a beaker glass containing 25 mL of MB dye with an initial concentration of 50 mg/L. This experiment was conducted at room temperature, and we examined various factors, including contact time, initial concentration, and temperature.

To assess the kinetics of adsorption, the contact time was varied by setting it at intervals of 10, 20, 30, 60, and 120 min. To determine the maximum adsorption capacity, we modified the initial concentration of MB dye within 25 to 200 mg/L (25, 50, 100, 150 to 200 mg/L). Additionally, to investigate the activation energy of the adsorption process, we conducted experiments at different temperatures, specifically 30, 40, and 50°C.

Throughout all our adsorption tests, a stirring rate of 200 rpm was maintained. After the completion of the reaction, we filtered the solution and analyzed the remaining dye concentration using a UV-Vis spectrophotometer set at 660 nm. The results were expressed as adsorption capacities (q_e), representing the amount of dye adsorbed per gram of adsorbent in milligrams per gram ($mg \cdot g^{-1}$). Furthermore, we calculated the adsorption efficiency (%) of the adsorbent using the provided equation below [17-19]:

$$q_e = \left(C_i - C_f\right).V/W \quad (1)$$

where C_i, C_f, V and W are the initial dye concentration, the remaining dye concentration after time t, the dye solution volume, and the adsorbent weight, respectively.

Results and Discussion

Physico-chemical Properties

The wavelength dispersive X-ray fluorescence (WDXRF) was used to determine the elements inside MG sample. The result shows that the MG(300) and MGO(300) contain the major elements such as calcium (Ca), phosphorus (P), and potassium (K). The manganese (Mn), iron (Fe), copper (Cu), nickel (Ni), and zinc (Zn) as various transition metal elements were also found inside the MG(300) and MGO(300) samples. The highest composition for all MG and MGO samples is Ca. Worth noting that K is the second highest element in MG(300) and MG(500), but the K composition decreases a lot after H_2O_2 activation. Besides, it is noted that no Ni composition is detected in MG(500) and no sulfur in MGO(500). Both Ni and sulfur are relatively low for MG(300) and MGO(300) too. All elements were listed in Table 1.

Table 1. Elements analysis of MG(300), MGO(300), MG(500) and MGO(500) obtained using WDXRF

Element (wt%)	MG(300)	MGO(300)	MG(500)	MGO(500)
P	4.10	4.23	5.25	8.19
S	0.30	0.60	1.40	-
K	17.50	2.10	17.30	5.35
Ca	73.10	84.20	72.10	81.30
Mn	1.60	2.80	1.50	1.80
Fe	0.88	1.50	0.80	1.10
Cu	0.20	0.32	0.13	0.19
Ni	0.01	0.10	-	0.21
Zn	0.44	0.67	0.44	0.45

Figure 1 displays the FTIR spectra of four distinct samples: (a) MG(300), (b) MGO(300), (c) MG(500), and (d) MGO(500), with measurements spanning the range of 400 to 4000 cm^{-1}. In all these spectra, it is observed that absorption bands within the 2500 to 3600 cm^{-1} region, which correspond to the stretching vibration of hydroxyl (O-H) groups found in the organic compounds within the materials. Additionally, there are bands at 2920 and 2846 cm^{-1}, which can be attributed to the symmetric and asymmetric stretching modes of aromatic and aliphatic C-H sp^3 groups within the organic template [20-21]. Notably, Figure 1(a) and (b) exhibits two evident absorption bands at 2920 and 2846 cm^{-1} at a lower carbonization temperature (300 ^oC), however, the intensities for Figure 1(c) and (d) inconspicuous as the carbonization temperature increases to 500 ^oC, aligning with the reduction of carbon content from aromatic and aliphatic compounds in MG. Furthermore, the absorption bands at 1054 and 598 cm^{-1} are identified, which associating with the stretching mode of SO_3^{2-} and the deformation of SO_2, respectively. Another band at 877 cm^{-1} represented for the acidic phosphate group (HPO_4^{2-}) [22]. Additionally, the absorption band at 1653 cm^{-1} is linked to the presence of calcium ions (Ca^{2+}). Lastly, the absorption bands within the 450 to 650 cm^{-1} range are related to the vibration of M-O (M= Fe, Mn, Cu, Ni, and Zn) bonding.

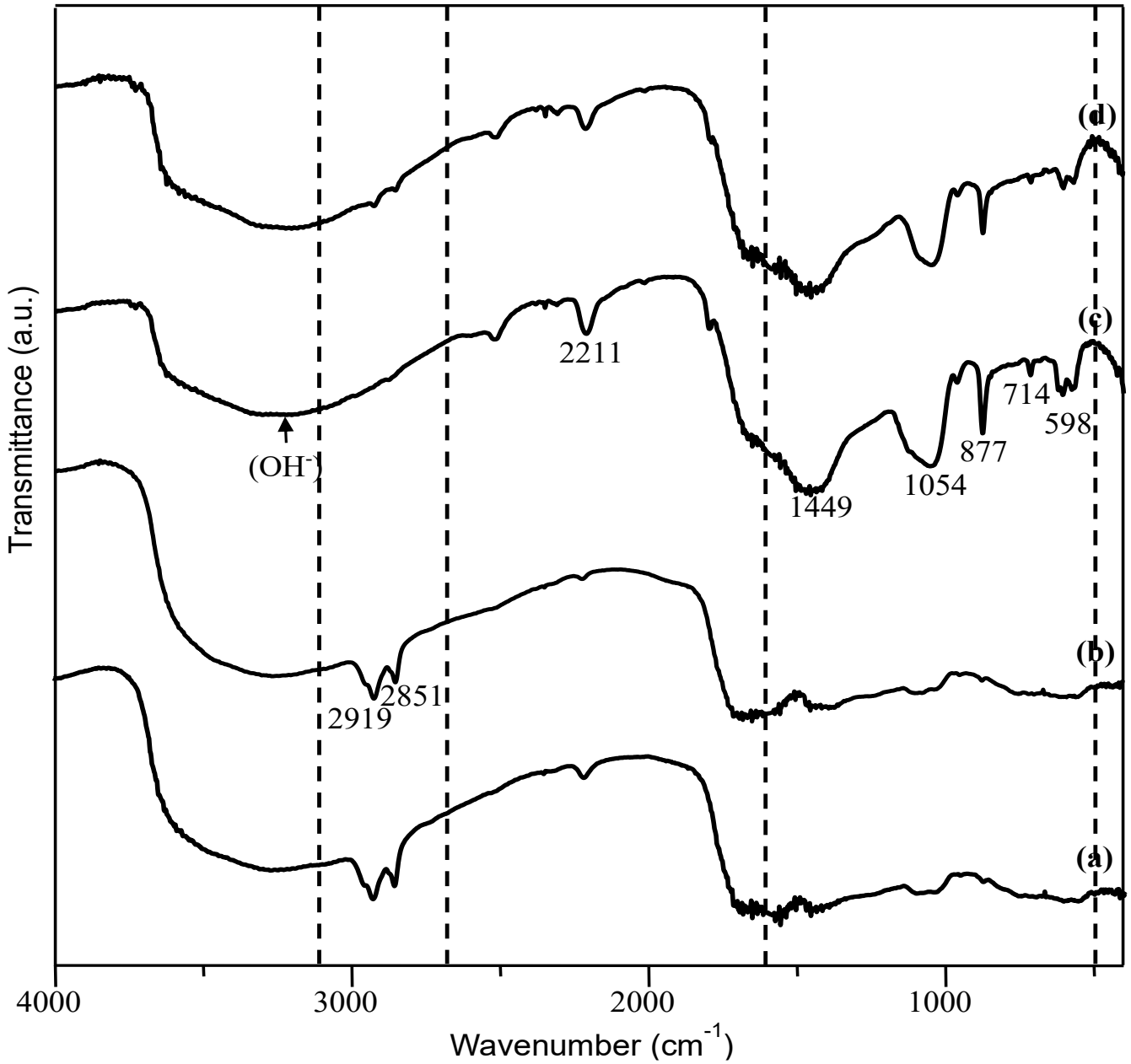

Figure 1. FTIR spectra of (a) MG(300), (b) MGO(300), (c) MG(500) and (d) MGO(500)

Figure 2 shows the XRD pattern of (a) MG(300), (b) MGO(300), (c) MG(500) and (d) MGO(500) are measured in 2θ at 7−60 °. The amorphous carbon composed of aromatic carbon sheets oriented in a considerably random fashion in Figure 2 (a and b) was proven by the broad but weak diffraction peaks in the XRD patterns at 2θ angles of 15−30°. Figure 2 (c and d) exhibits the amorphous carbon composed of aromatic carbon sheets no appear, which proves an increase of carbonization temperature increase from 300 to 500 °C can cause the release of aromatic carbon. Based on XRD pattern, activation carbon-derived maggot with H_2O_2 is inaffected to its crystallinity. It was proven XRD pattern a to b similar and c to d also no change. All XRD patterns show the slim peak at 2θ = 30°, that indicate the CaO and $Ca(OH)_2$ crystal. The peak intensity increases when the carbonization temperature was increased.

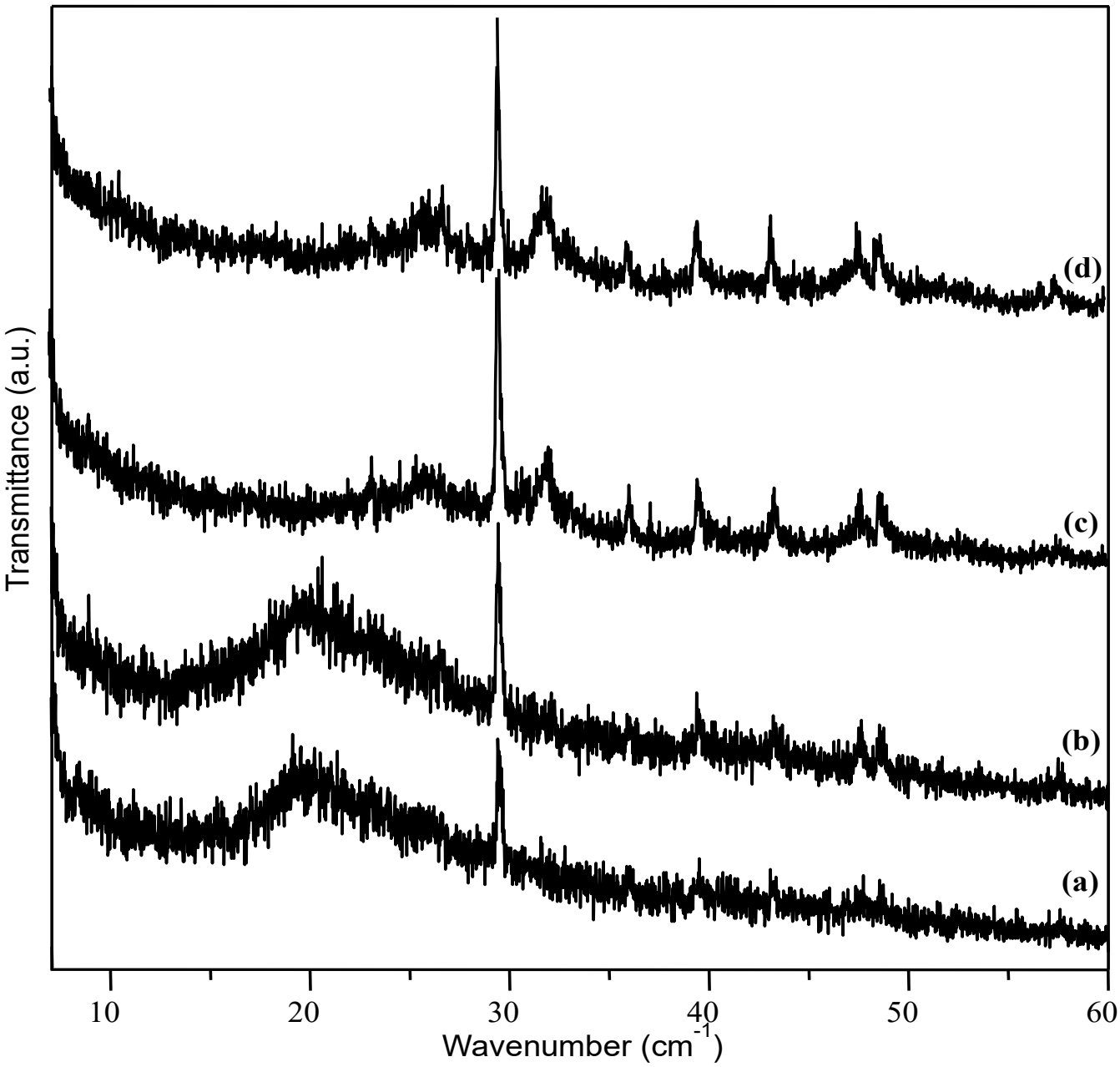

Figure 2. XRD pattern of (a) MG(300), (b) MGO(300), (c) MG(500) and (d) MGO(500)

Figure 3 shows the SEM images of (a) MG(500) and (b) MGO(500). The surface morphologies of both samples are porous and roughness. Both MG(500) and MGO(500) depict mesoporous structures, which evidenced by nitrogen adsorption-desorption isotherm. The effect of H_2O_2 treatment causes the surface morphology filled with more particulates than before.

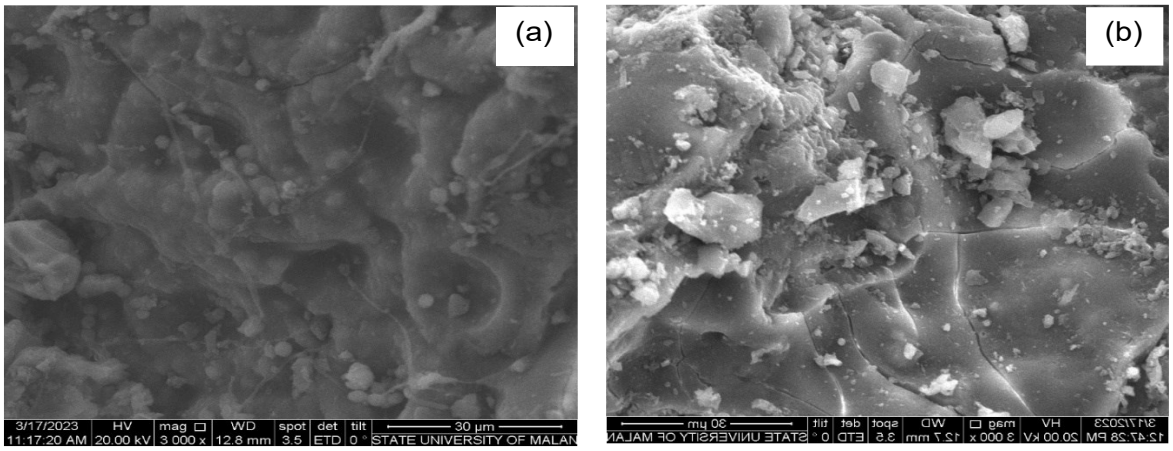

Figure 3. SEM Images of (a) MG(500) and (b) MGO(500)

An analysis of the surface area, pore volume, and pore structure for all the samples using nitrogen adsorption-desorption isotherms was conducted. Figure 4 illustrates the nitrogen adsorption-desorption isotherms for four different materials: (a) MG(300), (b) MGO(300), (c) MG(500), and (d) MGO(500). Notably, all of these isotherms fall under Type IV in the IUPAC classification, a characteristic classification for mesoporous materials. Mesoporous materials exhibit a distinctive feature characterized by a knee in the isotherm. Additionally, these isotherms display hysteresis loops in specific relative pressure ranges: ~0.01-0.95 for MG(300), ~0.2-0.95 for MGO(300), ~0.4-1.0 for MG(500), and ~0.4-1.0 for MGO(500). The surface area, pore volume, and mean pore size data are presented in Table 2. Notably, all the samples possess pore sizes exceeding 2 nm, indicating the presence of uniformly sized mesopores.

It is observed that the pore volumes are increased after H_2O_2 activation, proven by the increase of pore volumes of MG(300) and MGO(300), 0.0133 to 0.0354 cm^3/g, and MG(500) and MGO(500), from 0.0511 to 0.0616 cm^3/g. On the other hand, the mean pore sizes for MG(500) and MGO(500) are increased, from 5.434 to 7.402 nm. However, a drop could be observed for MG(300) and MGO(300) pore sizes, which is possibly caused by the tiny pores of MGO(300) are blocked by particulates. This is in agreement with the SEM image of MGO(500) showing more roughness surface after the H_2O_2 activation. The MG(500) and MGO(500) were carbonized at a higher temperature, which resulting in a larger pore size, thus particulate blocking is less likely to occur.

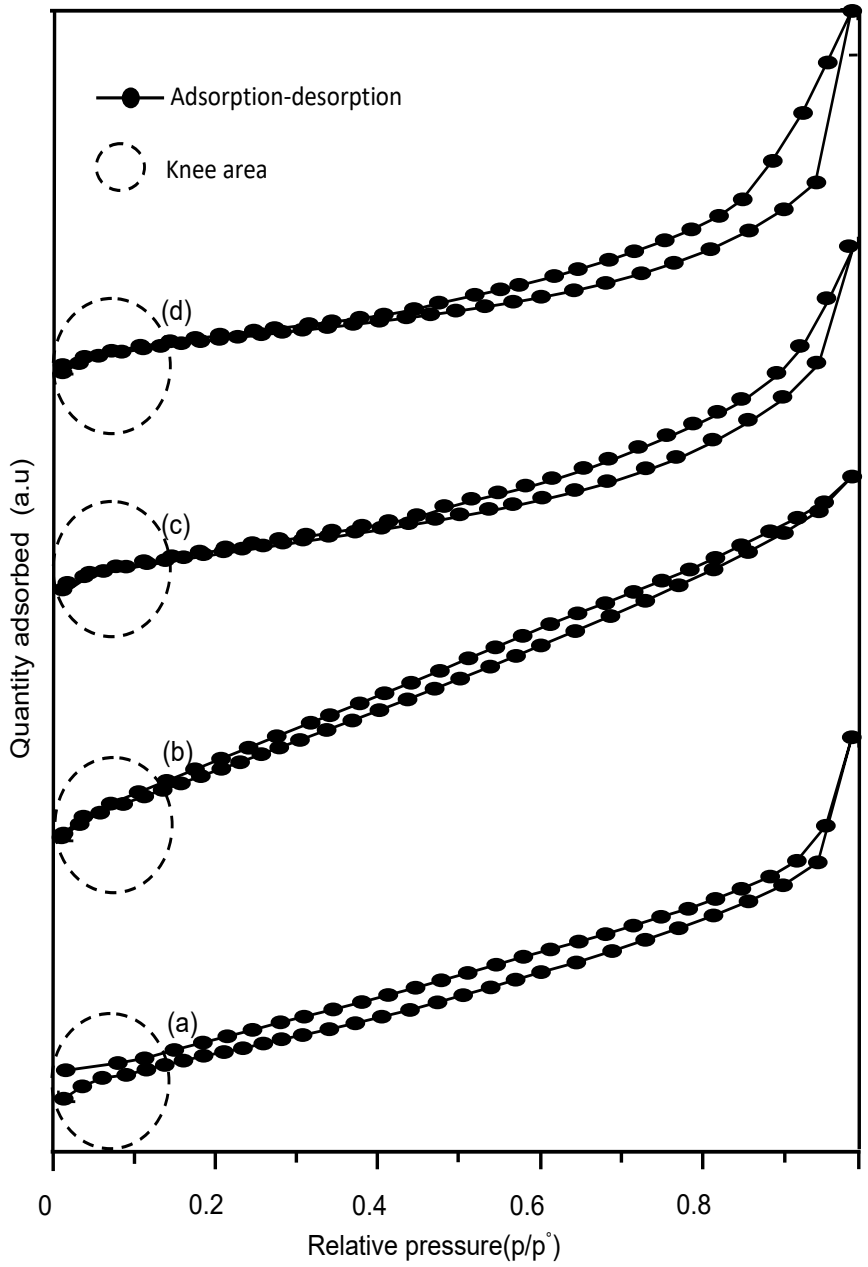

Figure 4. The physisorption isotherms of (a) MG(300), (b) MGO(300), (c) MG(500) and (d) MGO(500)

Table 2. BET surface area, pore volume and mean pore **size** of the samples

Samples	BET surface area (m^2/g)	Pore Volume (cm^3/g)	Mean pore size (nm)
MG(300)	6.237	0.0133	4.258
MGO(300)	27.911	0.0354	2.540
MG(500)	18.822	0.0511	5.434
MGO(500)	16.647	0.0616	7.402

Adsorption of Kinetic

Figure 5 depicts the influence of contact time on the adsorption of MB on four distinct adsorbents: (a) MG(300), (b) MGO(300), (c) MG(500), and (d) MGO(500). These findings reveal that equilibrium adsorption was achieved within 50 min with adsorption percentage of 76.5% for MG(500) and 96.1% for MGO(500) adsorbents. Whereas for MG(300) and MGO(300) adsorbents achieved the equilibrium adsorption after 60 min in adsorption process with adsorption percentage 65.7% and 91.1%, respectively. Interestingly, all the adsorbents exhibited rapid MB adsorption within the initial 10 min of contact time, showcasing impressive adsorption capacities: 6.33 mg.g^{-1} for MG(300), 11.07 mg.g^{-1} for MG(500), 16.41 mg.g^{-1} for MGO(300), and 17.13 mg.g^{-1} for MGO(500). Beyond this initial period, changes in adsorption capacity showed a gradual increase until equilibrium was attained. It is worth noting that MG(300) exhibited a lower adsorption capacity compared to MG(500), MGO(300), and MGO(500), primarily due to the physical properties of MG(500), MGO(300), and MGO(500), which possess higher surface areas. Furthermore, the presence of polar functional groups, like OH, COOH, and C=O, on the surface of MGO(300) and MGO(500) play a pivotal role for the adsorption of MB dye in aqueous solutions.

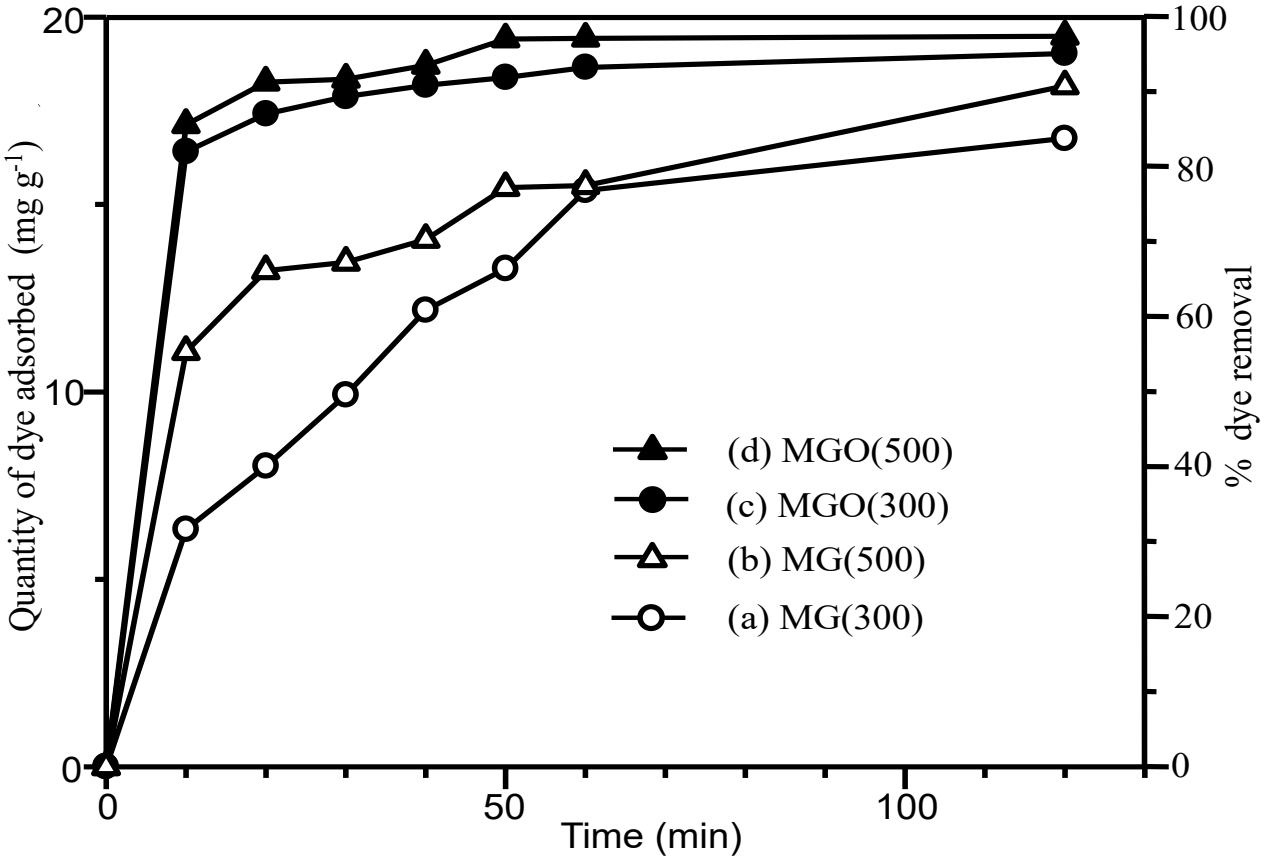

Figure 5. Kinetics parameters of (a) MG(300), (b) MG(500), (c) MGO(300) and (d) MGO(500)

The adsorption kinetics of dye adsorption was investigated by the pseudo-first order (PFO) and pseudo-first order (PSO) models. The PFO equation can be expressed with the following Lagergren equation [20, 23]:

$$\frac{dq}{dt} = k_{1,ad}(q_e - q) \quad (2)$$

After integration was obtained as:

$$log\ (q_e - q_t) = log\ q_{e,cal} - \frac{k_f}{2.303} t \quad (3)$$

where k_f, q_e and q_t were the rate constant (g/mg·h) for the PFO adsorption, the amounts of dye adsorbed per gram of adsorbent (mg/g) at equilibrium and any t time. $q_{e,\,cal}$ and k_f were determined from slope and intercept in the graph of t versus log ($q_e - q_t$).

The PSO kinetic model was expressed by Ho, Y. S., and McKay, G with the equation[24-25]:

$$\frac{dq}{dt} = k_{2,ad}\,(q_e - q)^2 \quad (4)$$

$$\frac{t}{q_t} = \frac{1}{k_2 q_{e.cal}^2} + \frac{t}{q_{e.cal}} \quad (5)$$

where $q_{e,\,cal}$ and k_2 were determined from slope and intercept in the graph of t versus t/q_t. k_2 is the rate constant for the PSO adsorption.

The experimental adsorption data were fitted with kinetics and isotherm models to obtain useful knowledge of the adsorption process and behavior [26]. The resulting fitting and the associated variables are specified in Table 3. Based on the given information, it appears that the PSO model provides a better fit to experimental data, as indicated by the higher R^2 values compared to the PFO model. The calculated q_e values using the PSO model also tend to be closer to the experimental q_e values. The PSO indicated a chemical process and assumed that the rate of adsorption is dependent on the square of the amount of adsorbate on the surface [27-28].

Table 3. The PFO and PSO kinetic parameter for MB dye adsorption of MG(300), MGO(300), MG(500) and MGO(500)

Adsorbents	PFO				PSO			
	q_e calculation (mg g^{-1})	q_e experiment (mg g^{-1})	k_1 (g $mg^{-1}min^{-1}$)	R^2	q_e calculation (mg g^{-1})	q_e experiment (mg g^{-1})	k_2 (g $mg^{-1}min^{-1}$)	R^2
MG(300)	1.076	16.766	0.0372	0.942	18.692	16.766	0.0030	0.949
MGO(300)	7.792	19.032	0.0545	0.846	19.193	19.032	0.0326	0.999
MG(500)	11.814	18.161	0.0281	0.851	18.587	18.161	0.0067	0.985
MGO(500)	11.646	19.488	0.0892	0.911	19.607	19.488	0.0456	0.999

Several crucial thermodynamic parameters were determined, including activation energy (E_a), free energy (ΔG), enthalpy (ΔH), and entropy (ΔS), through experiments conducted at varying temperatures. The detailed thermodynamic parameters for the adsorption process onto the MGO(500) adsorbent can be found in Table 4. Specifically, the investigation of activation energy (E_a) for the adsorption process was conducted, with our analysis concentrating exclusively on the MGO(500) adsorbent employed at temperatures of 25, 40, and 50°C. The calculation of E_a is performed utilizing the Arrhenius equation [29-30]:

$$\ln k = \ln A - \frac{E_a}{RT} \quad (6)$$

k is the rate constant. E_a is Arrhenius activation energy (kJ mol^{-1}), T is temperature of the adsorption medium (K). R is the ideal gas constant (8.314 J $mol^{-1}K^{-1}$), and A is the Arrhenius factor. The slope of graph ln k versus 1/T was used to calculate E_a. The E_a of adsorption process onto MGO(500) was obtained 5.807 kJ mol^{-1}.

The Van't Hoffs equation was used to determine the value of ΔH and ΔS of adsorption:

$$\log K_c = \frac{\Delta S}{2.303R} + \frac{\Delta H}{2.303RT} \quad (7)$$

The equilibrium constant (K_C) was which calculated by the equation:

$$K_C = \frac{C_1}{C_2} \quad (8)$$

The pertinent variables at play are denoted as follows: T, representing the absolute temperature in Kelvin; R, signifying the universal gas constant, a value of 8.314 J $K^{-1}mol^{-1}$; C_1, which stands for the quantity of dye adsorbed per unit mass of adsorbent; and C_2, representing the concentration of dye within the aqueous phase. To elucidate alterations in entropy (ΔS) and enthalpy (ΔH) during the adsorption phenomenon, a pivotal analytical tool involves the construction of a linear plot. The natural logarithm of the equilibrium constant (ln K_C) is correlated against the reciprocal of temperature, represented as 1,000 divided by the absolute temperature (1,000/T). These thermodynamic parameters are subsequently computed based on this plot's gradient (slope) and y-intercept (intercept). An affirmative ΔS value indicates an augmentation in the degree of disorder or randomness intrinsic to the ongoing process. Conversely, a negative ΔH value indicates that the adsorption process is characterized as exothermic, releasing heat into its surroundings.

For an adsorption process to be spontaneous can be identified by the negative value of Gibbs free energy (ΔG) at each temperature. The ΔG value was determined by the equation:

$$\Delta G = \Delta H - T\Delta S \quad (9)$$

Table 4. The value of ΔH, ΔS and ΔG for adsorption process onto MGO(500)

Dyes	ΔH (kJ/mol)	ΔS (kJ/mol K)	ΔG (kJ/mol)			E_a (kJ/mol)
			25 °C	40 °C	50 °C	
MB	−5.143	0.435	−18.106	−18.759	−19.194	5.807

Effect of Initial Concentration

The impact of varying initial concentrations of MB dye on the adsorption process is presented in Figure 6. Notably, we observed that the adsorption capacity of the dye increased proportionally with higher initial dye concentrations. When reaching equilibrium, the adsorption capacity of the dye ranged from 8.3 to 36.7 $g \cdot g^{-1}$ as the initial dye concentration was raised from 25 to 200 mg L^{-1}. This phenomenon suggests that an elevated initial concentration can serve as a driving force, effectively overcoming all mass transfer resistances encountered by dye molecules during their transition from the aqueous phase to the solid phase. This results in an amplified equilibrium sorption until saturation is reached. This trend aligns with previous findings, where a similar pattern was reported in the adsorption of MB on various plant parts (roots, stems, and leaves) at MB concentrations ranging from 0.80 to 8.0 mg L^{-1} [23].

The Langmuir adsorption isotherm was used to determine the maximum adsorption capacity of MGO(500) adsorbent. The Langmuir isotherm was only focused the monolayer sorption onto a surface and is determined by equation:

$$\frac{C_e}{q_e} = \frac{1}{Q_{max}} C_e + \frac{1}{Q_{max} \cdot b} \quad (10)$$

where Q_{max} and b are the maximum adsorption capacity and bonding energy of adsorption which calculated of the slope and intercept of the graph of $\frac{C_e}{q_e}$ versus C_e.

The Freundlich isotherm model was used to investigate the heterogeneous site energies of sorption that determined with equation:

$$\ln q_e = \ln K_F + \left(1/n\right) \ln C_e \quad (11)$$

There are two key parameters used in this study, i.e. K_F and n, which play significant roles in characterizing adsorption. KF represents the Freundlich constant, reflecting the adsorption capacity, while n stands for adsorption intensity. These parameters were determined by analyzing the intercept and slope of the plot generated from the natural logarithm of equilibrium adsorption (ln q_e) against the natural logarithm of the initial concentration (ln C_e). This analysis helps us compute KF (measured in mg g^{-1}) and n (expressed in (L $mg^{-}1)1/n$). KF is instrumental in quantifying the adsorption capacity, while n offers insights into the favorability of the adsorption process. When the value of n exceeds 1, it signifies a favorable adsorption condition.

The Langmuir and Freundlich adsorption isotherms were employed to characterize the interaction between dyes and the MGO(500) adsorbent. To remove MB using the MGO(500) adsorbent, various dye concentrations (ranging from 25 to 200 mg L^{-1}) were mixed with 0.0625 mg of the sorbent. This mixture was stirred at 300 rpm for 30 min at room temperature. The constants Q_{max} and b were obtained from the Langmuir isotherm, which amounted to 37.9 mg g^{-1} and 0.2215, respectively. Meanwhile, the constants K_F were determined, n, and R^2 from the Freundlich isotherm, resulting in values of 12.577 and 4.037 for K_F and n, respectively.

The K_F value suggests that the MB adsorption process is heterogeneous, occurring on the surface of the MGO(500) adsorbent through a multi-layer adsorption mechanism. Furthermore, the n values for the MB adsorption process are greater than 1, indicating favorable adsorption of both dyes onto the MGO(500) adsorbent.

The Langmuir adsorption isotherm gives a higher correlation coefficient of 0.998, so it is a better fit than Freundlich adsorption isotherm. You can find the complete set of results in Table 5.

Table 5 Langmuir and Freundlich isotherm models for adsorption of MB dye on MGO(500)

Adsorbent	Langmuir isotherm			Freundlich isotherm		
	Q_{max}	b	R	K_F	n	R^2
MGO(500)	37.879	0.2215	0.998	12.577	4.037	0.899

Conclusion

In this study, the feasibility of employing BSF larvae (Hermetia illucens) as a cost-effective source of carbon adsorbents was investigated. The procedure involved the modification of BSF through a carbonization process, followed by activation with H_2O_2, resulting in a promising and economically viable adsorbent for the removal of MB from aqueous solutions. The adsorption capacities of these materials were rigorously assessed through batch experiments, with an initial MB concentration of 100 mg/L, conducted at room temperature. It was observed that the sorption capacity of MGO (Modified BSF with H_2O_2) surpassed that of the MG adsorbent. This was substantiated by the values obtained from the equilibrium with adsorption percentage and sorption experiments (q_e, exp), which were measured at 65.7% and 6.33 mg·g^{-1} (MG(300)), 76.5% and 11.07 mg·g^{-1} (MG(500)), 91.1% and 16.41 mg·g^{-1} (MGO(300)), and 96.1% and 17.13 mg·g^{-1} (MGO(500)). Notably, the adsorption processes for MB in aqueous solutions, employing all the adsorbents, adhered to the pseudo-second-order kinetics model. The rate constants for this process were determined to be 0.0030 g mg^{-1} min^{-1} (MG(300)), 0.0326 g mg^{-1} min^{-1} (MG(500)), 0.0067 g mg^{-1} min^{-1} (MGO(300)), and 0.0456 g mg^{-1} min^{-1} (MGO(500)). Moreover, it was established that the adsorption process onto MGO(500) operated through a multi-layer adsorption mechanism. This observation aligns well with the findings of the Freundlich isotherm model, characterized by n values exceeding 1. Additionally, based on Langmuir isotherm model, the maximum adsorption capacity of MGO(500) was determined to be 37.879 mg·g^{-1}. Importantly, the thermodynamic parameters indicated a negative value of -18.686 kJ mol^{-1} for free energy, signifying the spontaneous nature of the MB adsorption process on MGO(500).

Conflicts of Interest

The author(s) declare(s) that there is no conflict of interest regarding the publication of this paper.

Acknowledgment

The authors gratefully acknowledge research grant Fakultas Keguruan dan Ilmu Pendidikan, Universitas Mulawarman TA. 2023 by contract number: 830/UN17.5/PG/2023

References

[1] Jayanegara, A., Novandri, B., Yantina, N., Ridla, M. (2017). Use of black soldier fly larvae (Hermetia illucens) to substitute soybean meal in ruminant diet: An in vitro rumen fermentation study. *Veterinary World, 10*(12), 1439-1446.

[2] Amrul, N. F., Ahmad, I. K., Basri, N. E. A., Suja, F., Jalil, N. A. A., Azman, N. A. (2022). A review of organic waste treatment using black soldier fly (hermetia illucens). *Sustainability 14*(8), 4565.

[3] Diener, S., Zurbrügg, C., Gutiérrez, F. R., Nguyen, D. H., Morel, A., Koottatep, T., Tockner, K., (2011). Black soldier fly larvae for organic waste treatment-prospects and constraints. *Proceedings of the Waste Safe, 2*, 13-15.

[4] Antonov, A., Ivanov, G., Pastukhova, N., Bovykina, G. (2019). Production of chitin from dead Hermetia Illucens. *IOP Conference Series: Earth and Environmental Science, 315*, 042003.

[5] Ratchai, E., Luengchavanon, M., Techato, K. A., Limbut, W., Chotikhun, A., Voo, N. Y. (2023). Characteristics of carbon from chitin-coated LiFePO 4 and its performance for lithium ion battery. *BioResources, 18*(3), 4399-4412.

[6] Micaela, T., Elena, T., Guarnieri, A., Salvia, R., Scieuzo, C., Hahn, T., Zibek, S., Gagliardini, A., Panariello, L., Coltelli, M. B., Bonis, A. D., Falabella, P. (2022). Characterization of chitin and chitosan derived from Hermetia illucens, a further step in a circular economy process. *Scientifc Reports 2022*, *12*(6613),1-1 7.

[7] Hameed, B. H., Din, A. M., Ahmad, A. L. (2007). Adsorption of methylene blue onto bamboo-based activated carbon: Kinetics and equilibrium studies. *Journal of Hazardous Materials, 141*(3), 819-825.

[8] Avom, J., Mbadcam, J. K., Noubactep, C., Germain, P. (1997). Adsorption of methylene blue from an aqueous solution on to activated carbons from palm-tree cobs. *Carbon, 35*(3), 365-369.
[9] Senthilkumaar, S., Varadarajan, P. R., Porkodi, K., Subbhuraam, C. V. (2005). Adsorption of methylene blue onto jute fiber carbon: kinetics and equilibrium studies. *Journal of Colloid and Interface Science, 284*(1), 78-82.
[10] Verma, A. K., Dash, R. R., Bhunia, P. (2012). A review on chemical coagulation/flocculation technologies for removal of colour from textile wastewaters. *Journal of Environmental Management, 93*(1), 154-168.
[11] Alventosa-deLara, E., Barredo-Damas, S., Alcaina-Miranda, M. I., Iborra-Clar, M. I. (2012). Ultrafiltration technology with a ceramic membrane for reactive dye removal: Optimization of membrane performance, *Journal of Hazardous Materials, 209*, 492-500.
[12] Yu, S. L. M., Ma, M., Qi, M., Lü, Z., Gao, C. (2010). Impacts of membrane properties on reactive dye removal from dye/salt mixtures by asymmetric cellulose acetate and composite polyamide nanofiltration membranes. *Journal of Membrane Science, 350*(1-2), 83-91.
[13] Kordouli, E., Bourikas, K., Lycourghiotis, A., Kordulis, C. (2015). The mechanism of azo-dyes adsorption on the titanium dioxide surface and their photocatalytic degradation over samples with various anatase/rutile ratios. *Catalysis Today, 252*, 128-135.
[14] Kuang, Y., Zhang, X., Zhou, S. (2020). Adsorption of methylene blue in water onto activated carbon by surfactant modification. *Water, 12*(2), 587.
[15] Ushakova, N., Dontsov, A., Sakina, N., Bastrakov, A., Ostrovsky, M. (2019). Antioxidative properties of melanins and ommochromes from black soldier fly hermetia illucens. *Biomolecules, 9*(408), 1-12.
[16] Souza, P. R. d., Ribeiro, T. M. d. C., Lôbo, A. P., Tokumoto, M. S., Jesus, R. M. d., Lôbo, I. P. (2020). Removal of bromophenol blue anionic dye from water using a modified exuviae of Hermetia illucens larvaeas biosorbent. *Environ Monit Assess, 192*(197), 1-16.
[17] Giri, A. K., Patel, R., Mandal, S. (2012). Removal of Cr(VI) from aqueous solution by Eichhornia crassipesroot biomass-derived activated carbon. *Chemical Engineering Journal,* 185-186, 71-81.
[18] Peng, Q., Yu, F., Huang, B., Huang, Y. (2017). Carbon-containing bone hydroxyapatite obtained from tuna fish bone with high adsorption performace for Congo red. *The Royal Society of Chemistry, 17*, 26968.
[19] Kusumawardani, R., Nurhadi, M., Wirhanuddin, Gunawan, R., Nur, H. (2019). Carbon-containing Hydroxyapatite obtained from fish bone as low-cost mesoporous material for methylene blue adsorption. *Bulletin of Chemical Reaction Engineering & Catalysis, 14*(3), 660-671.
[20] Wanyonyi, W. C., Onyari, J. M., Shiundu, P. M. (2014). Adsorption of congo red dye from aqueous solution using roots of eichhornia crassipes: Kinetic and equilibrium studies. *Energy Procedia, 50*, 862-869.
[21] Geng, W., Nakajima, T., Takanashi, H., Ohki, A. (2009). Analysis of carboxyl group in coal and coal aromaticity by Fourier transform infrared (FT-IR) spectrometry. *Fuel, 88*(1), 139-144.
[22] Jaber, H. L., Hammood, A. S., Parvin, N. (2017). Synthesis and characterization of hydroxyapatite powder from natural Camelus bone. *Journal of the Australian Ceramic Society, 54*(1), 1-10.
[23] Wanyonyi, W. C., Onyari, J. M., Shiundu, P. M. (2013). Adsorption of methylene blue dye from aqueous solution using eichhornia crassipes. *Bulletin of Environmental Contamination and Toxicology, 91*, 362-366.
[24] Mahmoodi, N. M., Kharramfar, S., Najafi, F. (2011). Amine-functionalized silica nanoparticle: Preparation, characterization and anionic dye removal ability. *Desalination, 279*, 61-68.
[25] Ho, Y. S., McKay, G. (1999). Pseudo-second order model for sorption processes. *Process Biochemistry, 34*, 451-465.
[26] Siraorarnroj, S., Kaewtrakulchai, N., Fuji, M., Eiad-ua, A. (2022). High performance nanoporous carbon from mulberry leaves (Morus alba L.) residues via microwave treatment assisted hydrothermal-carbonization for methyl orange adsorption: Kinetic, equilibrium and thermodynamic studies. *Materialia, 21*(101288).
[27] Widiyowati, I. I., Nurhadi, M., Hatami, M., Yuan, L. S. (2020). Effective TiO2-Sulfonated Carbon-derived from Eichhornia crassipes in the removal of methylene blue and congo red dyes from aqueous solution. *Bulletin of Chemical Reaction Engineering & Catalysis, 15*(2), 476-489.
[28] Nurhadi, M., Widiyowati, I. I., Wirhanuddin, Chandren, S. (2019). Kinetic of adsorption process of sulfonated carbon-derived from eichhornia crassipes in the adsorption of methylene blue dye from aqueous solution. *Bulletin of Chemical Reaction Engineering & Catalysis, 14*(1), 17-27.
[29] Pathania, D., Sharma, A., Siddiqi, Z. M. (2016). Removal of congo red dye from aqueous system using Phoenix dactylifera seeds. *Journal of Molecular Liquids, 219*, 359-367.
[30] Yang, L., Zhang, y., Liu, X., Jiang, X., Zhang, Z., Zhang, T., Zhang, L. (2014). The investigation of synergistic and competitive interaction between dye Congo red and methyl blue on magnetic $MnFe_2O_4$. *Chemical Engineering Journal, 246*, 88-96.